Kovove Mater. 59 2021 51–57
DOI: 10.4149/km_2021_1_51

Evolution of inoculation thermal analysis and solidification morphology of compacted graphite iron

S. Ai, Z. Xu*, Z. Liu, H. Song, A. Wang, L. Zhang, Z. Han, G. Gao, D. Li, D. Shi**

School of Materials Science and Engineering, Harbin University of Science and Technology, Harbin 150040, Heilongjiang, P. R. China

Received 8 September 2020, received in revised form 30 October 2020, accepted 22 February 2021

Abstract

This paper describes one possible thermal analysis method to anticipate and control the inoculation effect during the solidification of CGI melt. Results show that 0.10–0.45 % ferrosilicon inoculation in the sample cup can promote the solidification morphology of the melt to evolve from hypoeutectic to eutectic or even low hypereutectic. With the stepwise more inoculant additions, the minimum eutectic temperature difference for the two stepwise additions decreases. The inoculation saturation value is basically reached in the 0.30 % inoculant sample cup, of which the minimum eutectic temperature increase is 5.3 °C compared with that of the original melt. When inoculated, the carbon potential and eutectic inoculation potential of the melt are improved. At 0.45 % inoculant, the melt can solidify in the form of low hypereutectic. In this case, the nodularity rate increases significantly to 34 %, and large particles of graphite nodule appear.

K e y w o r d s: CGI, inoculation effect, thermal analysis evaluation, cooling curve pattern, solidification characteristics

1. Introduction

Compacted graphite iron (CGI) has been recognized as a high-performance engineering material for engine components [1–3]. CGI is an intermediate grade of cast iron between gray and ductile iron, with vermicular shape graphite in the matrix. CGI's material properties combine above 70 % increased tensile properties compared to gray iron with the same matrix and a better thermal conductivity than ductile iron. During the last decade, an intensive effort has been dedicated to introducing CGI for truck engine components. In practical production, CGI's graphite microstructure is expressed in terms of percent nodularity of a few spherical graphite, and flake graphite is not allowed. In the component's key position, the microstructure of a two-dimensional polished surface of a CGI sample must contain a minimum of 80 % vermicular shape graphite and less than 20 % nodularity to ensure excellent comprehensive physical properties.

In CGI production, the goal is to get as close to the eutectic solidification point as possible to get as much carbon precipitating in the form of graphite as possible to fill out the shrinkage porosity without getting any cementite or exploded graphite [4]. The narrow production process window of CGI and the unexpected parameter changes may lead to a large deviation in the treating effect of one-step graphite vermicularization. As the last adjustment of molten iron state, inoculation will have an independent or even contradictory effect on the actual solidification morphology of the melt and the nodularity rate of graphite particles [5–7]. Due to a lack of knowledge about actual solidification behavior and inoculation mechanism in CGI, it is more difficult to produce sound cast components, mainly due to the control of shrinkage porosity defects [4, 8]. Therefore, in CGI foundry, it is often seen that there are shrinkage porosity defects and unqualified graphite shape castings.

For an industrial melt, the equilibrium Fe-C diagram does not represent the real solidification morphology at a given carbon content because the cooling rate and other dissolved elements that are not accounted for in the equilibrium conditions affect the

*Corresponding author: e-mail address: zyxu@hrbust.edu.cn
**Corresponding author: e-mail address: shidequan2008@163.com

Table 1. Chemical compositions of molten iron in experiments (wt.%)

Molten iron	C	Si	Mn	P	S	Cu	Cr	Ni	Mo	Sn	Mg	RE	*CE**
Base iron	3.79	1.31	0.317	0.027	0.016	0.185	0.028	0.009	0.0235	–	–	–	4.24
Ladle 1	3.79	2.11	0.325	0.029	0.010	0.347	0.027	0.007	0.0240	0.064	0.014	0.012	4.50
Ladle 2	3.69	2.18	0.321	0.024	0.012	0.360	0.026	0.008	0.0227	0.057	0.014	0.015	4.42
Ladle 3	3.71	2.14	0.314	0.024	0.010	0.691	0.028	0.008	0.0232	0.057	0.015	0.016	4.43

*Carbon equivalent $CE = C\% + (Si\% + P\%)/3$

Table 2. Chemical compositions of treating agents (wt.%)

Material	Mg	RE	Si	Ca	Al	MgO	Ba	Fe
Vermicularization wire of ø 13 mm	7.0–10.0	3.0–6.0	43.0–45.0	2.0–5.0	–	≤ 2.0	–	Bal.
Inoculation wire of ø 13 mm	–	1.0–1.5	54.0–56.0	2.0–2.5	0.5–1.0	≤ 2.0	5.0–6.0	Bal.

fields and temperatures in the diagram. Therefore, it is very unlikely that in a production process for CGI, the eutectic reaction occurs for a carbon equivalent of 4.3 % predicted by the Fe-C equilibrium diagram. Eutectic saturation degree (Sc) only exists in theoretical analysis. Due to the undercooling and metallurgical non-equilibrium state of molten iron, graphite and austenite can be solidified simultaneously in an extensive range of carbon content and temperature. Compared with other traditional measurement methods, thermal analysis allows the recognition of unique melt characteristics in real time. This allows the definition of cooling curve patterns that characterize the best melt quality for solidification characteristics. The true solidification morphology can only be indicated by the cooling curve of thermal analysis [9–11]. The purpose of this paper is to study the effect of inoculation thermal analysis in sample cup on the real solidification morphology of CGI melt under the standard production method and parameters of the complex shaped automobile CGI casting, and to determine the optimal thermal analysis curve pattern, to provide experimental support for the measurement and control of the vermicularization and inoculation state of melt and better adjustment of process variables.

2. Experimental procedure

The trials were executed during regular production in a foundry that uses middle frequency induction furnaces to melt. The wire feeding method for treatment and pouring is performed directly from the treatment ladle into the molds. The charging materials consist mainly of pig iron, scrap steel, returns, carbon riser, various intermediate alloys, etc. When the charging materials were totally melted down, and the temperature had risen to over 1500 ℃, a sample was poured for C, Si, and *CE* check by thermal analysis. Simultaneously, a chilled sample was poured for chemical composition analysis by emission spectrometry and C and S content determination by combustion method. The composition of molten iron was controlled according to Table 1.

Treatment was made by the wire feeding method in a 0.5-ton ladle. During the experiments, to ensure the standard absorption rate of Mg, vermicularization and inoculation should be carried out at the same time according to the proportion specified by the factory. The types and specifications of vermicularizing agent and inoculant cored wires are shown in Table 2. After vermiculation and inoculation treatment, a spectrometer sample, a chilled sample, and thermal analysis samples were taken from the same ladle melt. The cylindrical sample cup with a small inner chamber size of ø 25 × 50 mm^2 was used for thermal analysis, and its solidification time was about 90 s. A set of data collectors recorded the cooling temperature data. Six thermal analysis cups were poured simultaneously for each ladle of molten iron. The additive amount of ferrosilicon inoculant in six chambers was 0, 0.10, 0.20, 0.30, 0.40, and 0.45 % of the sample melt weight, respectively. To keep consistent with the actual production, the inoculant added to the bottom of the sample cup is taken from the powder in the inoculation cored wire, and the particle size is 80 mesh. A high concentration of silica makes the melt exothermal, and that it blends well. The test was repeated three times (for three ladles from the same base iron) to check the results' reliability. The chemical compositions from the chilled samples are also presented in Table 1. After cutting, mounting, and polishing, all the thermal analysis samples near the cups' hot node were later investigated by an optical microscope at the laboratory for metallographic evaluation. Image analyses were then performed on the samples to define the amount of nodularity by Image-Pro Plus software.

Table 3. Nomenclature and definition of the critical characteristic points on a CGI cooling curve and its first derivative

Designation	Signification
T_{AL} (℃)	Precipitation temperature of primary austenite
T_{GL} (℃)	Precipitation temperature of primary graphite
T_{EU} (℃)	Minimum eutectic temperature
R_E (℃ s^{-1})	Average eutectic recalescence rate
T_{ER} (℃)	Maximum eutectic temperature
T_S (℃)	Temperature at the end of solidification

Table 4. Main characteristic point values and graphite nodularity corresponding to cooling curves in Fig. 1

Inoculant additions (%)	Detailed data of characteristic point values of thermal analysis						Graphite area ratio (%)	Nodularity (%)
	T_{AL}/T_{GL} (℃)	T_{EU} (℃)	R_E (℃/s^{-1})	T_{ER} (℃)	ΔT (℃)	T_S (℃)		
0	1145.5	1134.3	0.63	1138.0	3.7	1082.5	11.17	8
0.10	1142.6	1136.0	0.87	1139.6	3.6	1081.4	14.34	17
0.20	1140.8	1138.4	0.50	1140.6	2.2	1082.1	15.26	23
0.30	1140.3	1139.6	0.38	1141.7	2.1	1081.5	16.53	12
0.40	1140.6	1140.6	0.52	1142.5	1.9	1079.9	15.39	7
0.45	1141.9	1141.8	0.19	1142.5	0.7	1084.6	18.92	34

3. Results and discussion

As seen in Table 1, the Cu content in ladle 3 CGI melt is higher than that in ladle 1 and ladle 2 to produce more pearlite in a matrix; carbon equivalent *CE* and other compositions are almost the same. Due to the very close compositions between CGI's three ladle melts, they are expected to have the same solidification behavior. They will be the same type of alloy when analyzed unless big differences between them are noted. As expected, the cooling curve pattern and evolution trend of each ladle of molten iron verified the above statement. The nomenclature and definition of some key characteristic points on the CGI cooling curve measured in the experiment as shown in Table 3.

The classic thermal analysis curves recorded in testing experiments from ladle 3 melt are presented in Fig. 1, where they are ordered according to their solidification morphology caused by the increase of inoculant content in the sample cup chamber, from the less hypoeutectic to hypereutectic. Important solidification characteristics are identified on the cooling curve. Table 4 shows the main characteristic point values on the test cooling curve. As shown, the cooling curve of the original molten iron in the sample cup without inoculant shows hypoeutectic solidification morphology. With the stepwise more ferrosilicon inoculant additions in the sample cup from 0.10 to 0.30 %, the primary austenite temperature T_{AL} decreases, and the carbon equivalent *CE* increases. This indicates that some silicon elements dissolve into the molten iron during inoculation in the sample cup of

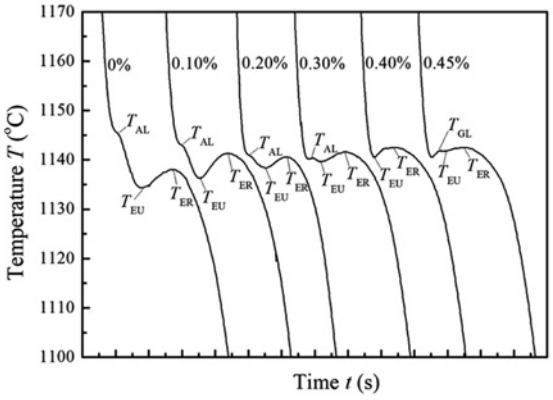

Fig. 1. Thermal analysis curve section on the liquid/solid transformation, showing the different solidification morphologies of the CGI melt affected by stepwise more additions of inoculant in the sample cup.

ferrosilicon alloy to play an alloying role. The increase of the minimum eutectic temperature (T_{EU}) indicates that the undercooling of molten iron is continuously decreasing. Eutectic solidification has a greater competitive advantage than austenite dendrite solidification. The maximum eutectic temperature T_{ER} keeps stable after a significant increase and the solidification temperature range of eutectic decreases and moves to a high-temperature region. At 0.40 % ferrosilicon addition, the primary austenite temperature T_L is equal to the minimum eutectic temperature T_{EU}, and the solidification state of vermicular graphite eutectic is

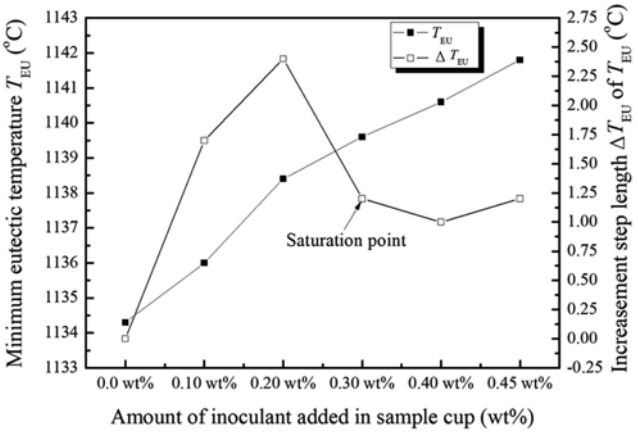

Fig. 2. Effect of inoculation in sample cup on undercooling level of eutectic solidification.

achieved. When the addition of ferrosilicon inoculation is further increased to 0.45 %, a small exothermic peak T_{GL} of primary graphite appears on the cooling curve of the molten iron sample. This is because the latent heat release of primary graphite is small. A large amount of eutectic latent heat is released during eutectic solidification, so there is another highest eutectic temperature T_{ER} peak after T_{GL}. Limited by the small sample mass of molten iron and the inoculation conditions in the sample cup, the smaller exothermic peak T_{GL} of primary graphite overlaps with the part of the highest eutectic exothermic peak T_{ER}.

However, the eutectic solidification time of hypereutectic solidification morphology is longer than that of hypoeutectic. Therefore, hypoeutectic curves of CGI are characterized in the liquid to solid transformation by having two main inflection points in the solidification phase (corresponding to liquidus of primary austenite and eutectic temperatures, respectively), where the second inflection has a much larger recalescence compared to that of ductile iron [10–12]. Eutectic solidification curves of CGI are characterized in the liquid to solid transformation by having only one inflection. Hypereutectic curves have again two inflections (corresponding to liquidus of primary graphite and eutectic temperatures). The first inflection has a smaller recalescence than the second one in this inoculation experiment carried out in the cup cavity of the thermal analysis sample. Another fact shows that the true carbon equivalent of the eutectic melt is higher than 4.43 %, and the eutectic temperature is about 1142 ℃. Therefore, the determination of solidification morphology of compacted graphite iron should always be done using the thermal analysis evaluation of melt after treatment and prior pouring.

Figure 2 shows the change of undercooling level of eutectic solidification with increased inoculant addition in the sample cup. It can be seen that the minimum eutectic temperature T_{EU} rises with the increase of inoculation level. However, it can be seen from the minimum eutectic temperature difference ΔT_{EU} value between the two cooling curves of adjacent stepwise more inoculant additions in the cup that in this experiment, with the increase of inoculant amount, it begins to increase significantly and reaches the maximum value of 2.4 ℃ at 0.20 % addition, and then reaches a saturation point value after decreasing at 0.30 % additional amount. This additional amount has made the melt sample reached a near eutectic solidification morphology. With the inoculant amount increase, the eutectic inoculation level reaches a stable value, and the solidification morphology further evolves into a eutectic and low hypereutectic state. Compared with ladle 1 and ladle 2, the inoculation thermal analysis effect of the ladle 3 melt is more significant. In addition, it can be seen from the above analysis that the actual *CE* content and eutectic inoculation level of the ladle 3 seem to be lower. The reason may be that, according to the normal regulations, a fixed amount of ferrosilicon is placed at the bottom of the ladle for pre-inoculation to improve the initial inoculation level of base iron. However, in the ladle 3 base iron, the tapping is relatively late, and the residence time in the furnace is longer, so the initial eutectic inoculation potential energy is reduced. Therefore, the final inoculation level of the melt is lower after the same treatment process. Finally, the inoculation effect in the thermal analysis sample cup is more obvious. Using additional cups that have stepwise more additions of inoculant can recognize between which cups the difference in minimum eutectic temperature is below the reference value for the saturation point. When that is found, the cup with the lower additions of the inoculant of the two cups compared will tell you how much inoculant should be added to the melt.

Figure 3 shows the metallographic picture of graphite in the center of the sample corresponding to the solidification state of the thermal analysis curve. Combined with the change of the average eutectic recalescence rate R_E in Table 4, it can be seen that inoculation affects the eutectic solidification kinetics of CGI. From the cooling curve of the sample cup without inoculant, it can be seen that the temperature of primary austenite is obviously high, which indicates that the carbon equivalent *CE* of molten iron is low. Under the influence of dissolved Mg, O, and S's contents in equilibrium with metallurgical reaction are very low. The eutectic nucleation and growth are complicated, which leads to a large undercooling. When the amount of inoculant is 0.10 %, the eutectic nucleus grows, and the average recalescence rate R_E increases from 0.63 ℃ s^{-1} to 0.87 ℃ s^{-1}. It can be seen from Fig. 3a that the graphite in the sample without inoculant is mostly a mixture of thin flakes and a small amount of spherical graphite, and the end of

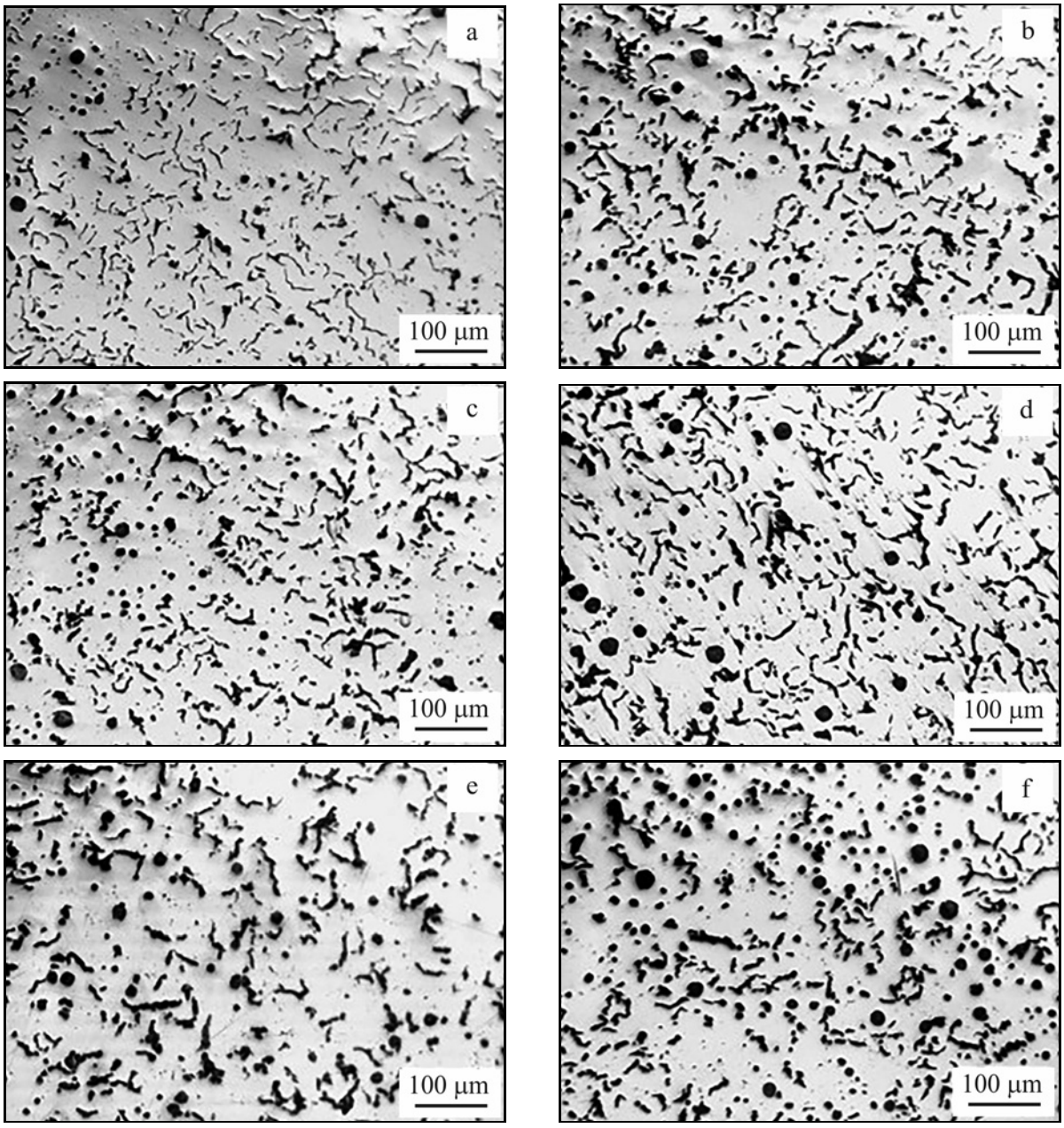

Fig. 3. Metallographic picture of graphite shape in the center of sample corresponding to solidification morphology of thermal analysis curve with different inoculant addition in sample cup, × 100: (a) 0 % addition, highly hypoeutectic state, (b) 0.10 % addition, less hypoeutectic state, (c) 0.20 % addition, less hypoeutectic state, (d) 0.30 % addition, near eutectic state, (e) 0.40 % addition, eutectic state, and (f) 0.45 % addition, hypereutectic state.

the bent graphite flake is slightly sharp, and the percentage content of graphite area is only 11.17 %.

In contrast, the graphite flakes in Fig. 3b become shorter and thicker, the ends become round and blunt. The number of graphite nodules increases, and the graphite area percentage reaches 14.34 %. According to the theory of non-equilibrium eutectic region, 0.10 % ferrosilicon inoculation can significantly improve the eutectic nucleation of molten iron in the sample cup, which makes the carbon equivalent of the true eutectic point decrease, and the carbon equivalent *CE* of the melt also increases greatly, so the carbon potential increases significantly. In the eutectic rapid solidification stage, the eutectic crystallization rate and graphite area percentage increase significantly.

With the further increase of inoculant addition, the average eutectic recalescence rate R_E decreases to 0.38 ℃ s^{-1} before reaching the true eutectic solidification state (corresponding to 0.30 % inoculant addition). In the eutectic solidification morphology (related to 0.40 % inoculant addition), the average eutectic recalescence rate R_E increases again to 0.52 ℃ s^{-1}.

The main reason for this trend is that with the further increase of inoculation level, the eutectic nucleation and growth basically reach an equilibrium level (the maximum eutectic temperature T_{ER}), and the average eutectic recalescence rate R_E decreases. In the eutectic solidification state, the average eutectic recalescence rate R_E increases due to eutectic austenite and graphite simultaneous precipitation. The eutectic solidification tends to be in an equilibrium state; the coupling and dissociation growth mode of vermicular graphite and austenite gradually takes the dominant position. As a result, the vermicular graphite particles and the graphite area ratio increase, while the nodularity rate decreases slightly. Therefore, the near eutectic and eutectic solidification morphology is considered the best solidification mode of CGI. During hypereutectic solidification, the average recalescence rate of the first primary graphite precipitation peak is $0.70\,℃\,s^{-1}$, resulting from graphite crystallization exothermic. Due to the partial overlap with the initial exothermic peak, the average recalescence rate of eutectic appears to be $0.19\,℃\,s^{-1}$, which may be lower than the actual rate. In the hypereutectic solidification state, the graphite area ratio reaches the maximum, but the nodularity rate is too high to meet the requirements, and a small number of large graphite particles appear.

4. Conclusions

In this paper, under the standard production method and process parameters of complex shape automobile CGI castings, the influence of inoculation thermal analysis in the sample cup on the real solidification morphology of CGI melt is studied, and the optimal thermal analysis curve pattern is determined. Combined with the metallographic analysis of graphite morphology, the specific conclusions are as follows:

(1) The evolution of the solidification morphology of compacted graphite iron can be revealed by incubation thermal analysis in the sample cup. With the stepwise inoculating additives, the cooling curve pattern changes from less hypoeutectic to eutectic and even low hypereutectic.

(2) Depending on the real carbon equivalent and especially the undercooling (inoculation potential) of the melt, it is possible to have a hypoeutectic solidification for *CE* values well above the theoretical eutectic point carbon equivalent of 4.3 %. The solidification morphology determined should always be done using thermal analysis evaluation of the melt after treatment and before pouring.

(3) With the prolongation of the holding time in the furnace, the molten state of base iron, especially the inoculation and nucleation potential, decrease. After conventional treatment, the eutectic undercooling degree of the melt is relatively large. When the carbon equivalent is low, the graphite particles will not be vermicularized well. According to the thermal analysis with stepwise more additions of inoculant in the sample cup, it is expected to realize the measurement and control of the real inoculation demand of melt.

Acknowledgement

The authors gratefully acknowledge the financial support of the State Key Laboratory of Engine Reliability.

References

[1] M. Tholl, A. Magata, S. Dawson, Thinner and lighter engine blocks for passenger car produced in high quality compacted graphite iron, J. Jpn. Foundry Eng. Soc. 67 (1995) 898–905. doi:10.11279/imono.67.12_898

[2] S. Dawson, Compacted graphite iron – A material solution for modern diesel engine cylinder blocks and heads, China Foundry 6 (2009) 241–246. doi:10.4271/2011-01-1083

[3] B. Mrzygłód, G. Gumienny, D. Wilk-Kołodziejczyk, K. Regulski, Application of selected artificial intelligence methods in a system predicting the microstructure of compacted graphite iron, J. Mater. Eng. and Perform. 28 (2019) 3894–3904. doi:10.1007/s11665-019-03932-4

[4] A. K. Ramos, A. Diószegi, W. L. Guesser, C. S. Cabezas, Microstructure of compacted graphite iron near critical shrinkage areas in cylinder blocks, Int. J. Metalcast. 14 (2020) 736–744. doi:10.1007/s40962-019-00403-3

[5] A. Regordosa, U. de la Torre, A. Loizaga, J. Sertucha, J. Lacaze, Microstructure changes during solidification of cast irons: Effect of chemical composition and inoculation on competitive spheroidal and compacted graphite growth, Int. J. Metalcast. 14 (2020) 681–688. doi:10.1007/s40962-019-00389-y

[6] G. Alonso, D. M. Stefanescu, P. Larrañaga, R. Suarez, Graphite nucleation in compacted graphite cast iron, Int. J. Metalcast. 14 (2020) 1162–1171. doi:10.1007/s40962-020-00441-2

[7] J. C. Hernando, B. Domeij, D. González, J. M. Amieva, A. Diószegi, New experimental technique for nodularity and Mg fading control in compacted graphite iron production on laboratory scale, Metall. Mater. Trans. A 48 (2017) 5432–5441. doi:10.1007/s11661-017-4315-3

[8] J. C. Hernando, J. Elfsberg, E. Ghassemali, A. K. Dahle, A. Diószegi, The role of primary austenite morphology in hypoeutectic compacted graphite iron alloys, Int. J. Metalcast. 14 (2020) 745–754. doi:10.1007/s40962-020-00410-9

[9] R. Sillén, Finding the true eutectic point – An essential task for efficient process control of ductile iron, Keith Millis Symposium on Ductile Iron 2 (2008) 100–104.

[10] V. Anjos, C. A. Silva Ribeiro, Maximization and control of nodular iron melt's self-feeding characteristics to minimize shrinkage, Mater. Sci. Forum 925 (2018) 147–154. doi:10.4028/www.scientific.net/MSF.925.147

[11] V. Anjos, Use of thermal analysis to control the solidification morphology of nodular cast irons and reduce feeding needs. [Ph.D. Thesis]. Duisburg-Essen: University of Duisburg-Essen 2015.

[12] V. Anjos, C. S. Ribeiro, J. Cunhaand, C. Gomes, The use of thermal analysis to compare solidification pattern and evaluate performance of several inoculants in ductile iron, Proceedings of 71st World Foundry Congress, WFC (2014). ISSN: 1888-444X.